HI IN THE MILKY WAY

Selected Problems Illustrated by the Leiden/Dwingeloo Survey

W.B. BURTON, DAP HARTMANN, AND S.R.D. WEST

Leiden Observatory
P.O. Box 9513, Leiden, 2300 RA, The Netherlands

Abstract. Some of the principal problems which can be confronted with HI observations of our Galaxy are illustrated here by a selection of maps showing the disposition on the sky of HI emitting in particular velocity ranges. The data are from the new Leiden/Dwingeloo survey of the entire sky north of $\delta \geq -30°$, which has occupied the 25–meter radio telescope of the Netherlands Foundation for Research in Astronomy for a period of five years. The tendency of the general gas/dust correlation to involve some HI structures with quite anomalous velocities is illustrated by comparing some $\lambda 21$–cm data taken on a finer grid using the Arecibo 1000–foot telescope with IRAS data in the 100–micron band.

A survey of neutral atomic hydrogen in our Galaxy has been completed using the 25–meter radio telescope in Dwingeloo. The new observations span the entire sky down to $\delta = -30°$ with a true–angle grid spacing of $0.°5$ in both l and b. The spectral resolution of the survey was set by the spacing of 1.03 km s^{-1} between each of the 1024 channels of the DAS digital autocorrelation spectrometer; the effective kinematic range of the material covers velocities (measured with respect to the Local Standard of Rest) between -450 km s^{-1} and $+400$ km s^{-1}. The characteristic *rms* limit on the measured brightness–temperature intensities is 0.07 K.

The data of the Leiden/Dwingeloo survey represent an improvement over that of earlier large–scale surveys by an order of magnitude or more in at least one of the principal parameters of sensitivity, spatial coverage, or spectral resolution. The observational and correction procedures are discussed in detail by Hartmann (1994).

447
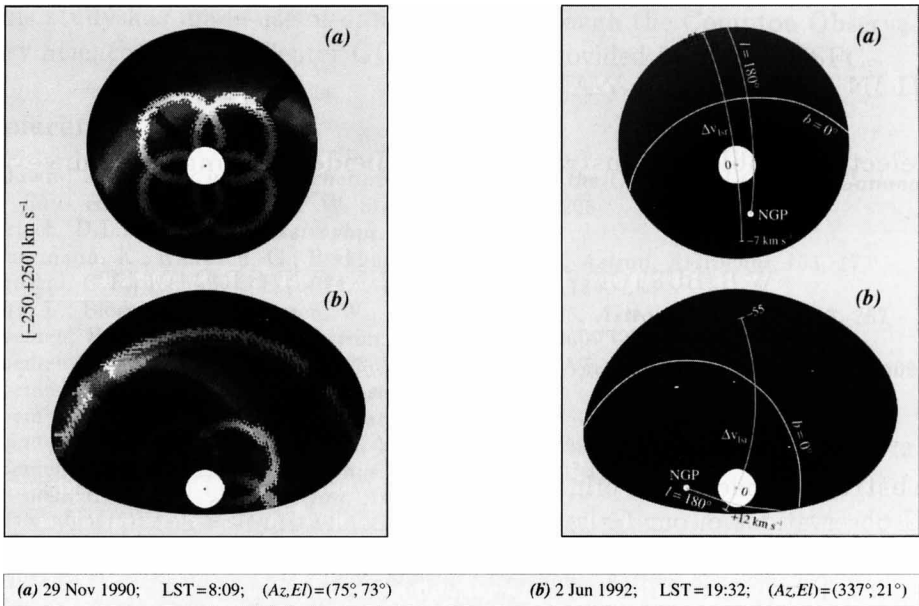
$$(l,b)=(160°, 50°)$$

Figure 1. Illustration of the differing manner in which the stray radiation contaminates two observations made toward the single direction $(l, b) = (160°, 50°)$. The right–hand panel indicates the orientation of the Milky Way when the two spectra were taken. The white circle corresponds to the extent of the near sidelobes; the center of the circle indicates the pointing of the main beam. The placements of the galactic equator $b = 0°$, and of the anticenter line $l = 180°$, are indicated for the two observations. The left–hand panel shows the differing fluxes perceived by the far sidelobe pattern; the sensitive features of this pattern fall on quite different parts of the Milky Way, and thus contribute quite differently to the resulting spectra, shown in Figure 2.

The Leiden/Dwingeloo survey is the first major survey to be largely corrected for contamination by stray radiation. (The sensitivity of the earlier Hat Creek surveys did not warrant the correction; the influence of stray radiation on the Bell Labs data was only minor because the horn reflector is not blocked by a feed–support structure.) The nature of the stray–radiation correction is illustrated by Figure 1; its importance is demonstrated by Figure 2. The correction involved convolving the empirically–determined response of the Dwingeloo antenna with the measured all–sky $\lambda21$–cm distribution. The correction was applied in collaboration with P. Kalberla and U. Mebold of the University of Bonn, using a modified version of the algorithm described by Kalberla *et al.* (1980). A detailed description of the application of the stray–radiation correction to the Leiden/Dwingeloo data is given by Hartmann *et al.* (1995).

The input HI sky comprised the Leiden/Dwingeloo survey itself, reduced in all aspects except for the stray–radiation correction. (The correction could therefore only be applied after the entire accessible sky had been observed.) For each individual HI spectrum entering the final survey, the input sky was separately consulted so that the situation at the date and time appropriate to each observation could be accounted for.

A model of the Dwingeloo antenna response was based on interferometric measurements made earlier by Hartsuijker *et al.* (1972), on holographic measurements of the telescopes of the Westerbork Synthesis Radio Telescope reported by van Someren Greve (1991), and on our own measurements of bright continuum sources. Corrections were determined separately for the far sidelobes (*FSL*) and for the near sidelobes (*NSL*). The *FSL* contribution is largely due to reflections off the feed–support structure and to radiation entering the feed directly, for example after reflection off the ground. The *NSL* contribution (taken as that perceived within 16° from the pointing axis of the main beam) is largely due to imperfections in the main beam of the antenna pattern.

The amount of emission impinging upon the sidelobes, and its velocity structure, depends on the perception of the Milky Way by the extended antenna pattern during the course of the observation. Figure 1 shows that this perception varies fundamentally for different times and dates, and for different observed positions. When a particular position is tracked, different portions of the Galaxy radiate into different regions of the antenna response pattern; these differing portions of the Galaxy will also have varying relative motions with respect to those characteristic of the particular direction in question. Figure 2 shows that two observations made toward the same direction on the sky can return spectra which differ in accordance with the manner in which the antenna response perceives the kinematics and structure of the HI sky.

The 0.07 K *rms* sensitivity limit on the brightness temperatures measured in the new material depends crucially on the success of the stray–radiation correction. This limit is about an order of magnitude less than the peak intensity characteristically entering the far sidelobes of the Dwingeloo antenna; more importantly, at lower $|b|$ it is typically two orders of magnitude less than the peak intensity entering the near sidelobes. The emission entering the *FSL* pattern is always a concern: because it is largely contributed by the HI disk near the galactic equator, its velocity structure typically extends over some 150 km s^{-1}. Figure 2 shows that in regions where the total HI emission is exceptionally weak, for example in the direction of the HI–deficient region in Ursa Major discussed by Lockman *et al.* (1986), the flux entering the sidelobes may be as strong as, or even in excess of, that received by the main beam of the telescope.
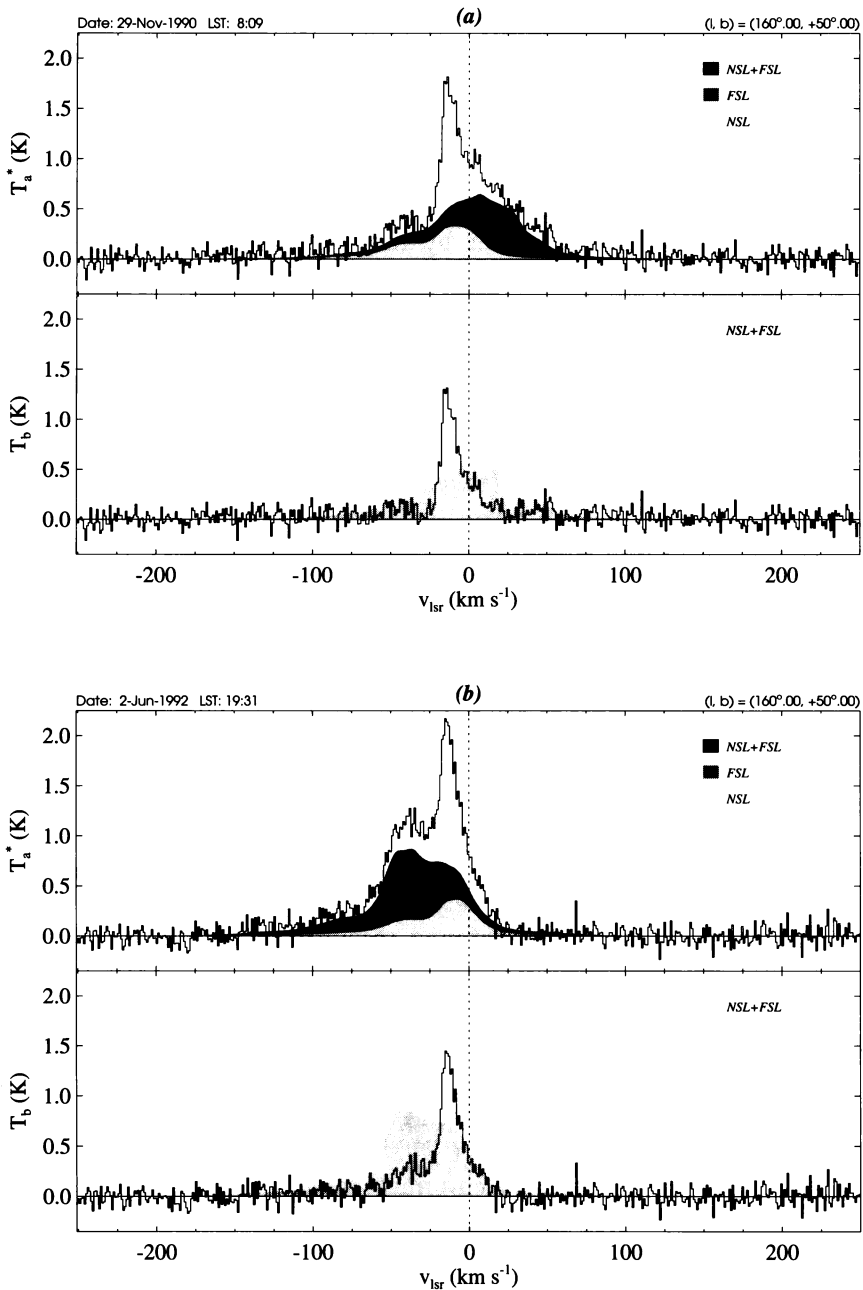
Figure 2. Illustration of the differing influence of stray radiation for two separate observations made on different dates toward the same direction, $(l, b) = (160°, 50°)$. (a) Observation made in November, 1990, at high elevation (73°). The *FSL* contribution is less prominent than in (b), because the spillover ring was directed toward the ground rather than toward the sky. (b) Spectrum observed in June, 1992, at an elevation of 21°. Here the spillover ring was pointing toward the sky. Figure 1 clarifies how *FSL* contamination entering the two spectra differs in intensity as well as in velocity.

The *NSL* contribution in a given direction shows little variation with time as the position of the main beam changes. The intensity of the near-sidelobe contamination can, however, be high. At low $|b|$, the contamination level is typically 10 K; although, unlike in the *FSL* case, the *NSL* contamination largely mimics the structure in the profile in question, correction for its total contribution is important to accurate determination of column depths, optical depths, and temperatures.

The Leiden/Dwingeloo HI survey is suited to a range of astronomical investigations; among those of most interest to us are the following:

• The survey is the first to embrace the kinematic regimes of the high– and intermediate–velocity clouds as well as that of gas at conventional velocities. There are a number of indications that the distinctions drawn between these regimes are arbitrary in important regards.

• Many dust cirrus features studied in the infrared have gas counterparts which can be traced to quite anomalous velocities. At least some interstellar cirri are evidently not quiescent objects with only modest energetics.

• The sensitivity and latitude coverage of the new data allow an improved description of the warp and flare of the gas layer in the outer Galaxy. It remains puzzling that the gas/dust correlation, which is so generally tight in the inner Galaxy and locally, apparently breaks down in the outer Galaxy; kinematic unraveling of the correlation as a function of galactocentric distance represents an important challenge.

• The relationship of HI intensity to interstellar extinction analyzed by Burstein and Heiles (1978) raised astrophysical questions which should be addressed again using modern data. Particularly important are the zero–point offset found in the relation between reddening and N_{HI}, and the variation in the gas–to–dust relationship found in different regions.

• Regions of exceptionally–low total N_{HI} in addition to the "hole" identified by Lockman *et al.* (1986) are being identified and their velocity characteristics studied. Regions of low N_{HI} are particularly of interest because of the role of interstellar HI in obscuring background X–rays.

• The extension of velocity information beyond the coverage and resolution available earlier will support determination of HI areal filling factors; important constraints can also be put on the more elusive volume filling factor. These factors are important to discussions of interstellar turbulence and scale–height maintenance, and of radiation penetration.

• The interstellar HI is largely marshaled into filamentary structures, variously named. Additional study of the form and motions of such structures will reveal the macroscopic energetics of the interstellar medium. Some structures have a kinematic span beyond the range of earlier data, suggesting a revision of the currently accepted energetics.

Figure 3.   Distribution over the plane of the sky of integrated HI emission contributed over the full velocity range -450 km s$^{-1} \leq v \leq +400$ km s^{-1}. Integration over such a large velocity range measures the total column depth (assuming optical thinness) and shows some aspects of galactic morphology, but suppresses crucial kinematic information.

$\Longrightarrow$

We illustrate a selection of these open problems (see also Burton, 1992) by representative slices through the Leiden/Dwingeloo HI data cube, supported by only cursory remarks. The deployment of astrophysically–relevant structures in a three–dimensional data cube is notoriously difficult to display (and, in consequence, also difficult to determine). Physical structures, not uncommonly with filamentary, or otherwise complicated, forms snake through any data cube constructed of orthogonal planes of l, b, and v; flat–plane cuts through such a data cube will not reveal the complete structural nature of the HI features. Nevertheless, such cuts are the most useful when displaying images of the entire sky. The slices shown here represent the distribution on the sky of integrated HI emission originating from the indicated velocity interval. (At high $|b|$, rectangular images are, of course, severely distorted; the principal advantage of rectangular images extending to the polar caps is that all the data can be displayed in a single map.)

Figure 3 shows the distribution of the total HI emission integrated over the full effective velocity range characterizing the new material, -450 km s$^{-1} \leq v \leq +400$ km s^{-1}. This map shows the sky coverage of the survey and displays some aspects of galactic morphology, but crucial kinematic information is suppressed by the large integration range.

Figure 4 shows the sky distribution of HI radiating between -90 km s^{-1} and -80 km s^{-1}. This range is particularly interesting because it falls between the regimes conventionally considered to separate the high–velocity–cloud objects from the intermediate–velocity ones. The distinction between these two classes of objects may be largely arbitrary; the high–velocity and the intermediate–velocity clouds merge rather continuously in velocity. The sky images at less extreme velocities show a smooth merger also of the IVCs with gas at conventional velocities; in fact, IVCs are not uncommonly associated with disturbances in the zero–velocity ambient gas, and there are some indications that the same conclusion holds for the HVCs. Perhaps the most important difference between the HVC and IVC objects is given by the failure to detect either dust emission or molecular emission from the HVC objects, despite substantial efforts to do so. IVCs, on the contrary, frequently have cirrus counterparts, and a few have associated molecular clouds; these few exceptions highlight the total lack of molecular–cloud and dust emission from the HVCs.

$-450 \leq V_{lsr} \leq +400 \text{ km s}^{-1}$

$-90 \leq V_{LSR} \leq -80 \text{ km s}^{-1}$
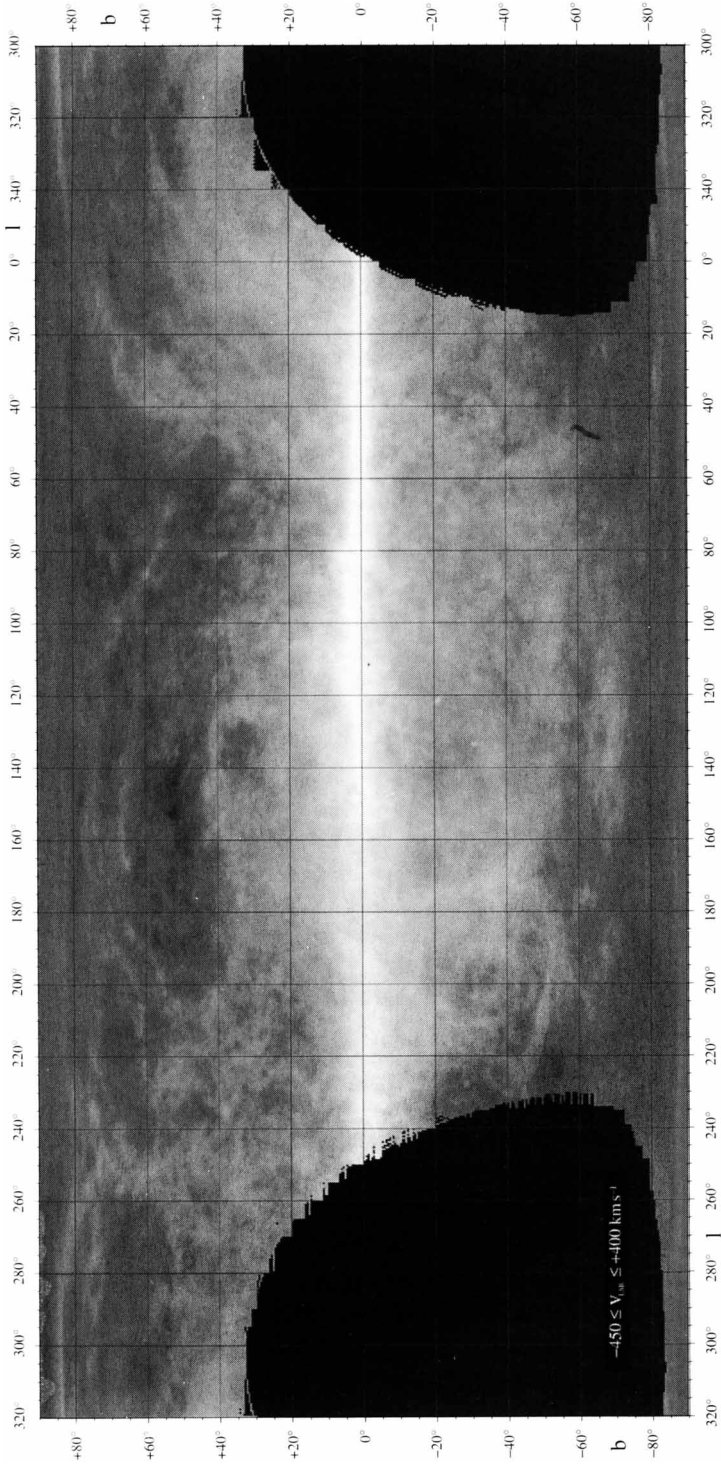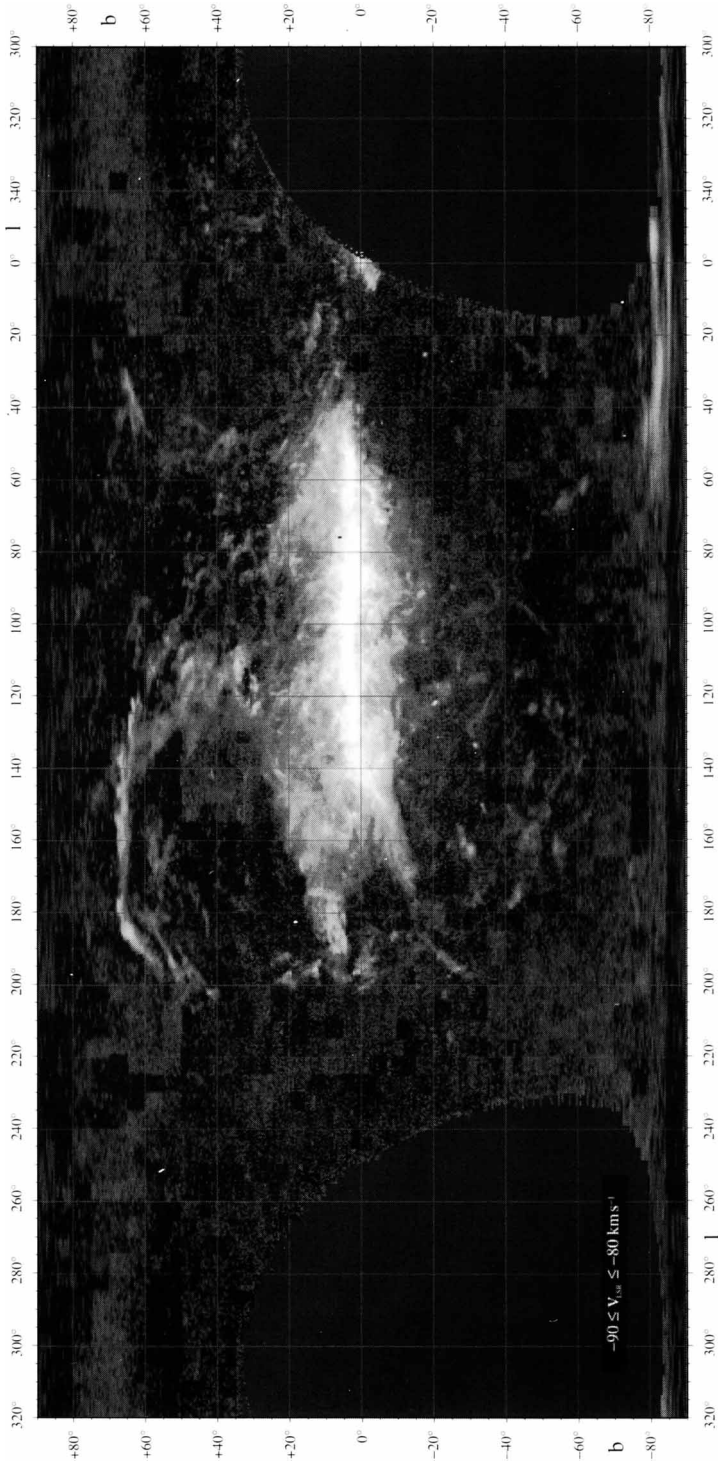
Figure 4. Sky distribution of HI column depths contributed over the velocity range -90 km s^{-1} $\leq$ v $\leq$ -80 km s^{-1}. Except close to the galactic equator, gas emitting at these velocities is largely contributed by high–velocity–cloud objects and by the more extreme intermediate–velocity clouds. Emission from the HVC Complex M is evident as the arc crossing the central upper portions of this map. $\Longleftarrow$
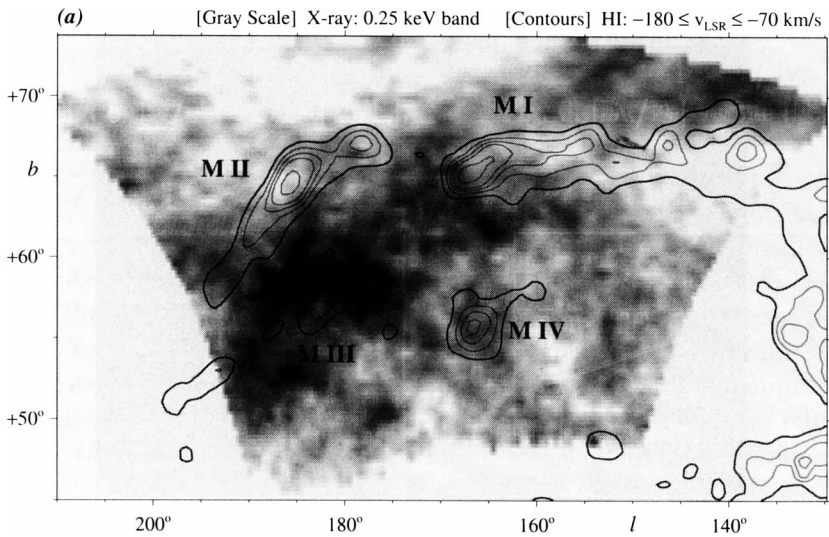
Figure 5. Grayscale plot of the ROSAT 1/4 keV X–ray image towards the HI HVC Complex M overlayed by contours showing the HI column–density distribution integrated between between -180 and -70 km s^{-1} (Herbstmeier *et al.* 1995). In this region of generally low N_{HI} column depths, enhanced X–ray emission is bounded by anomalous–velocity gas; the anticorrelation implies attenuation of the X–rays by foreground HI gas, and thus constrains the distances.

   The material in the -90 km s^{-1} $\leq$ v $\leq$ -80 km s^{-1} velocity range will enter studies of the galactic warp and flaring thickness. It is clear that measures of the thickness of the galactic gas layer, for example, or of the vertical line–of–sight velocity dispersion, must take account of possible distortion by the IVC emission.

   The question of the distance to the HVC gas remains a difficult one. Figure 5 shows that the HI in the HVC Complex M evidently attenuates the soft X–ray background measured by ROSAT at 1/4 keV. Herbstmeier *et al.* (1995) have compared the X–ray distribution with that of the HI gas radiating in various velocity ranges, and found that high–velocity clouds are responsible for some of the X–ray attenuations. If the distance of the

$-60 \leq V_{lsr} \leq -58$ km s^{-1}
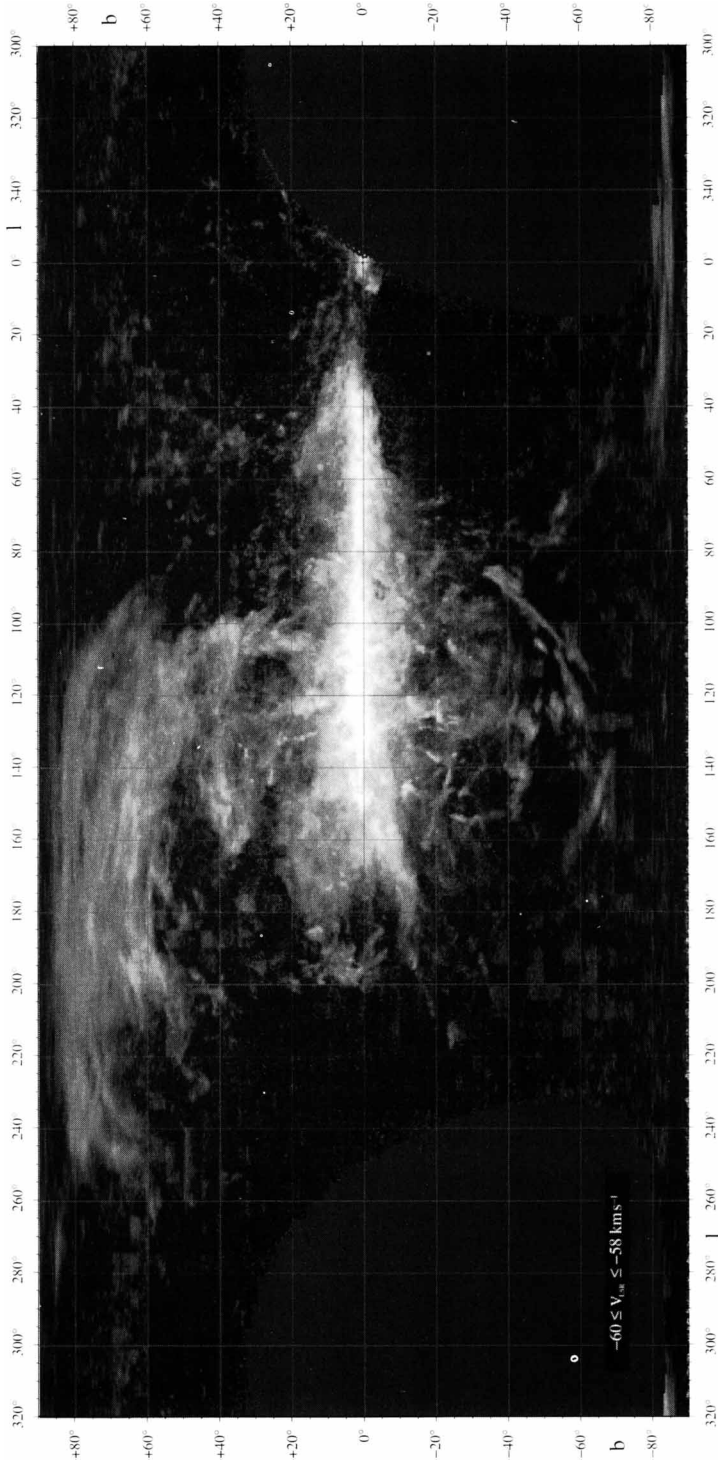
Figure 6. Distribution over the plane of the sky of HI column depths contributed over the narrow velocity range -60 km s$^{-1} \leq v \leq -58$ km s^{-1}. The so–called intermediate–velocity–cloud objects populating the higher $|b|$ region show a range of morphologies, still poorly understood in terms of filling factors, distance, origin, and energetics. Some, and maybe most, of these anomalous–velocity gas features have dust counterparts. ⇐

HVC complex has been correctly constrained to lie between 1.5 and 4.5 kpc, then the hot galactic corona extends at least several kiloparsecs from the galactic equator. Herbstmeier *et al.* also found evidence for an X–ray edge–brightening of the high–velocity clouds, suggesting that the clouds contribute to the heating of the corona.

Figure 6 shows the sky image of HI radiating in the narrow velocity range -60 km s$^{-1} \leq v \leq -58$ km s^{-1}. The situation at the moderate negative velocities (which were largely out of reach of the Hat Creek survey of Heiles and Habing, 1974) is evidently very interesting. Such velocity slices as the one shown in Figure 6 will provide substantial information on the various filling factors. The areal filling factor expresses the percentage of sky covered by HI structures, at specified velocities. The volume filling factor expresses the fraction of space occupied by the structures; requiring distance information, this factor will be more difficult to determine.

Data in the intermediate–velocity regime is also relevant to questions posed by the maintenance of the thickness of the galactic gas layer, especially that in the transition region between the lower halo and the conventional disk (see Dickey and Lockman 1990, and Lockman and Gehman 1991). Many of the "fast" clouds are in fact quite narrow in their σ_v measure. The concept of motions of separate entities forming an ensemble of structures only sparsely filling space, seems more realistic than the picture of a diffuse gas component at high $|b|$ with a large velocity dispersion. We note that the small scale–thickness and small line–of–sight σ_v measured in low $|b|$ in the inner Galaxy constrain a number of parameters of the IVC population.

The intermediate–velocity range, especially that at intermediate latitudes, is a rich source of information on the kinematic aspects of HI gas structures which are correlated with interstellar dust cirrus clouds. The kinematic structure can be unraveled by examining the gas/dust correlation as a function of velocity across the $\lambda21$–cm spectra of the associated gas (see Deul and Burton 1990, Burton *et al.* 1992, and West *et al.* 1995). All of the cirrus fields for which we have attempted kinematic unraveling using HI observations show relationships with the regime of intermediate–velocity gas. Evidently many cirri are not quiescent wisps, but involve substantial energetics.
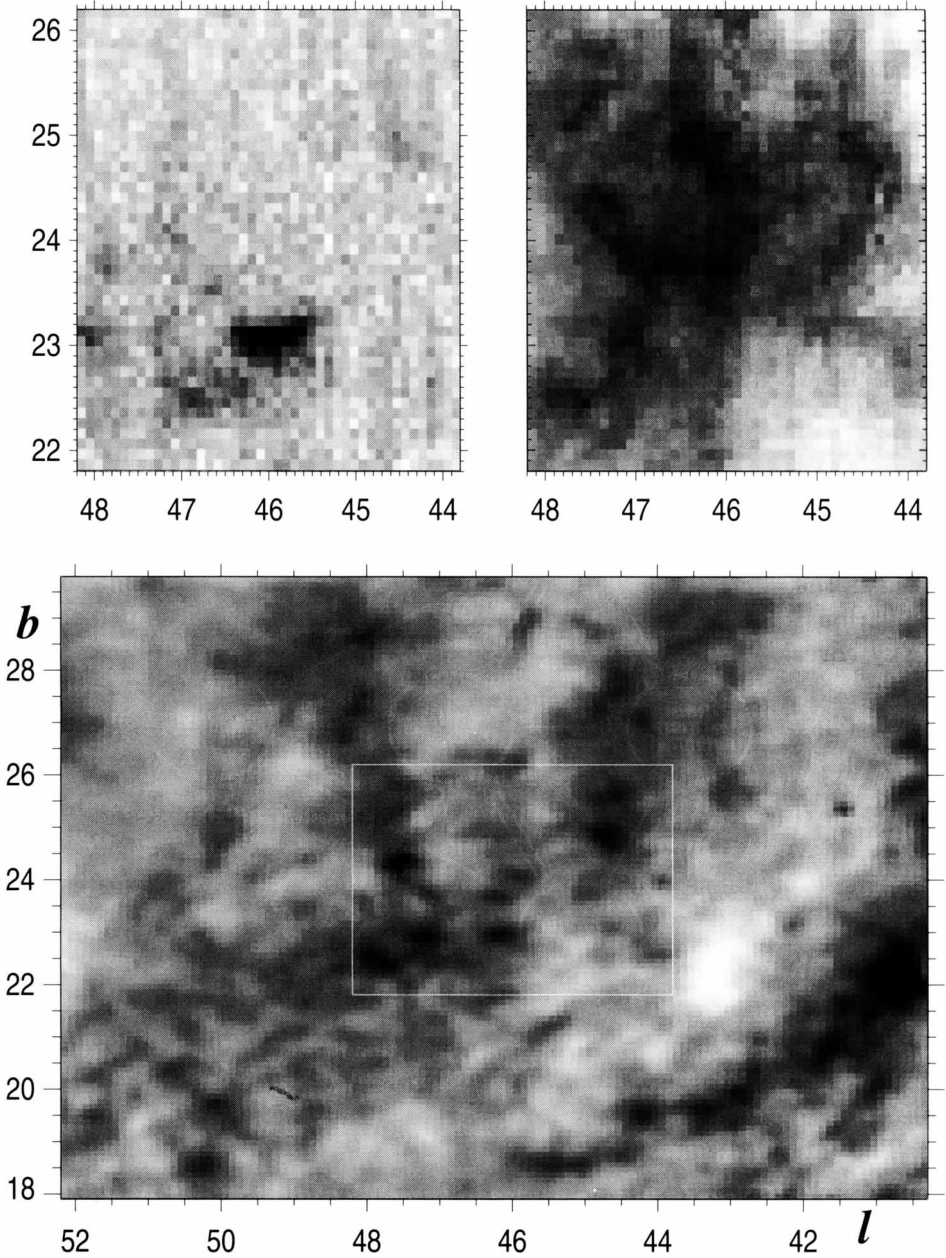
Figure 7. HI column densities, measured at Arecibo (West *et al.* 1995), corresponding to $\lambda21$–cm emission from the range -75 km s$^{-1} \leq v \leq -55$ km s^{-1} (left) and from the range -10 km s$^{-1} \leq v \leq +10$ km s^{-1} (right), compared with the IRAS 100–micron flux in the lower panel. (The boxed region in the lower panel delineates the extent of the Arecibo data.) The knot of HI emission at the anomalous velocities has a dust cirrus counterpart centered near $(l, b) = (46°, 23°)$. Cirrus filaments, with gas counterparts at velocities near zero, appear spatially associated with the IVC knot; if that association is a physical one, then the gas/dust association embraces more than 65 km s^{-1}. (Higher fluxes are blacker, for both the HI and the IR.)

Figure 7 shows the gas and dust emission from the vicinity of a cirrus feature centered near $(l, b) = (46°, 23°)$. The IRAS 100–micron map shows a dust feature with a filamentary morphology, centered on a knot of dust emission at $46°, 23°$. The dust filaments as well as the knot have gaseous counterparts, but at different velocities. The IR knot has a gas counterpart, centered near $v = -60$ km s^{-1}, radiating at velocities characteristic of a prototypical intermediate–velocity cloud. Furthermore, the HI column density corresponding to intensities integrated over the *conventional* velocity range -10 km s$^{-1} \leq v \leq +10$ km s^{-1} shows a deficiency of HI at the location of the IR knot. The gaseous counterparts of the filamentary structures, apparently focused toward the knot, radiate at the conventional velocities.

A satisfactory description of the $(l, b) = (46°, 23°)$ cirrus field will have to account for the relation of the HI IVC with its IR counterpart, as well as for the relationship of this pairing with the HI deficiency and apparent disturbance near zero velocity. It will also reckon with the appearance that filamentary dust features at modest velocities emanate from the position, and velocity, of the disturbance.

Figure 8 shows the sky image of HI radiating in the velocity range -40 km s$^{-1} \leq v \leq -38$ km s^{-1}; many of the points illustrated by Figure 6 pertain here also. We note in addition that some directions radiate more flux at these anomalous velocities than they do within, say, $|v| \leq 10$ km s^{-1}. Some of the individual HI features populating this velocity range have dispersions as small as $\sigma_v \simeq 1$ km s^{-1}. The measured widths are thus small enough to be relevant in estimating the kinematic temperature of HI clouds at high $|b|$. It appears promising to use the identification of narrow HI features (together with data on 100–micron excesses) as a finding chart for searching for high–latitude molecular clouds at these anomalous velocities.

Figure 9 shows the gas and dust emission from the vicinity of a cirrus feature centered near $(l, b) = (211°, 63°)$ in whose core Désert *et al.* (1990) found CO emission at -39 km s^{-1}. Molecular clouds at high latitude and at velocities differing from zero by more than 25 km s^{-1} are rare; only two are currently known in addition to the one found by Désert *et al.*, namely G90.0+38.6-25 (Heiles *et al.* 1988) and G135.3+54.5-45 (Mebold *et al.* 1989). Molecular gas associated with intense cirrus emission has frequently been observed, but generally confined to within about 5 km s^{-1} of zero velocity: the kinematic picture derived from most molecular emission associated with cirrus knots is a quiescent one.

The HI situation in the direction of the Désert *et al.* feature is particularly interesting. HI emission is intense near -40 km s^{-1}, and at these anomalous velocities it is well correlated with the 100–micron dust emission. The emission at velocities which would be associated with a quiescent

$-40 \leq V_{lsr} \leq -38$ km s^{-1}
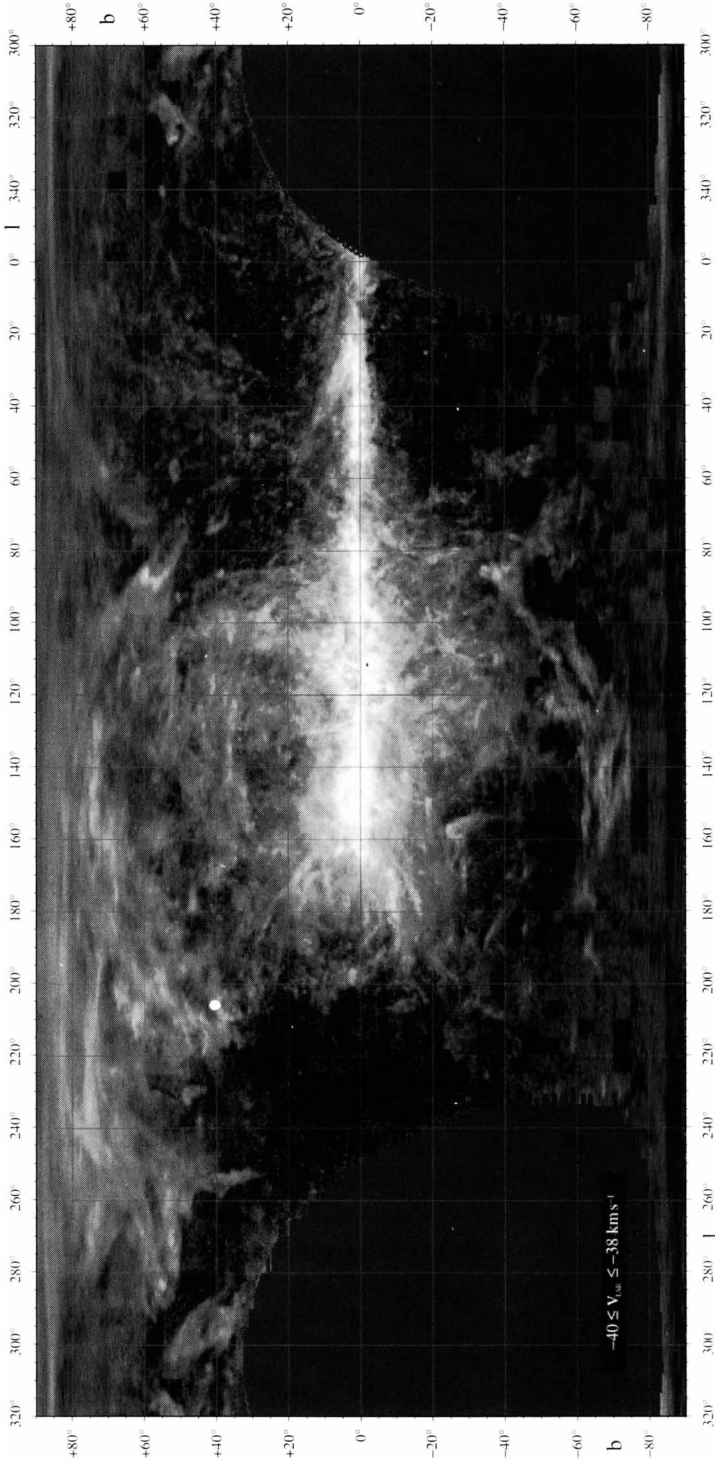
Figure 8. Distribution over the plane of the sky of HI column depths contributed over the narrow velocity range -40 km s$^{-1} \leq v \leq -38$ km s^{-1}. Some of the high–$|b|$ HI features are characterized by quite narrow velocity widths, as low as $\sigma_v \sim 1$ km s^{-1}. The small, narrow HI enhancement near $(l, b) = (211°, 63°)$ corresponds to the site where Désert *et al.* (1990) found a molecular cloud, one of only three molecular clouds known at $|v|$ more extreme than 25 km s^{-1}. The gas emitting at the anomalous velocities near -39 km s^{-1} dominates the total gas density budget in the direction of the associated cirrus structure. $\Longleftarrow$

ambient medium is exceptionally weak throughout the region. Just adjacent (on the north) to the IR knot and the molecular cloud, the total HI column depth approaches the exceptionally low values found in the direction of the Lockman *et al.* (1986) deficiency in Ursa Major. The HI spectral features associated with the IR knot and molecular cloud are quite narrow: the features near -39 km s^{-1} have Gaussian dispersions $\sigma_v \leq 1.4$ km s^{-1}. We note that the narrow measured dispersions are probably upper limits, not only because of the commonly–encountered possibility of blending of unrelated material, but also because the Arecibo data have not been corrected for stray–radiation effects: this correction systematically tends to render spectral features which are kinematically narrower than in the uncorrected case.

In addition to the HI feature emitting at -39 km s^{-1}, there is also a gaseous filament crossing the Arecibo map (in an unfortunately–sampled way, but confirmed in the Leiden/Dwingeloo data) just south of the Désert *et al.* cloud, at $b \sim 61°$, with $v \sim 0$ km s^{-1}. This conventional–velocity feature also has a dust counterpart. The IRAS 100–micron map shown in the lower panel of Figure 9 suggests that the two kinematic branches together form a single, shell–like structure; the HI data indicate kinematic continuity across some 40 km s^{-1}. The origin of the large total velocity extent of the shell–like structure which contains the peculiar–velocity molecular cloud remains a puzzle.

Most intermediate–velocity HI clouds have yet to be studied in detail. There are preliminary indications, however, that several of the characteristics of the gas/dust correlations pertaining for the $(l, b) = (211°, 63°)$ site may hold more generally, particularly the large total velocity span and the association of the anomalous–velocity occurrence with a perturbation in the conventional–velocity realm. We note that although intermediate–velocity HI features commonly trace extensive patterns over large angles on the sky, they also contain a great deal of small–scale structure, both spatially and kinematically. Many of these small–scale features are also quite cold, as indicated by the upper limits which can be placed on their velocity dispersions.
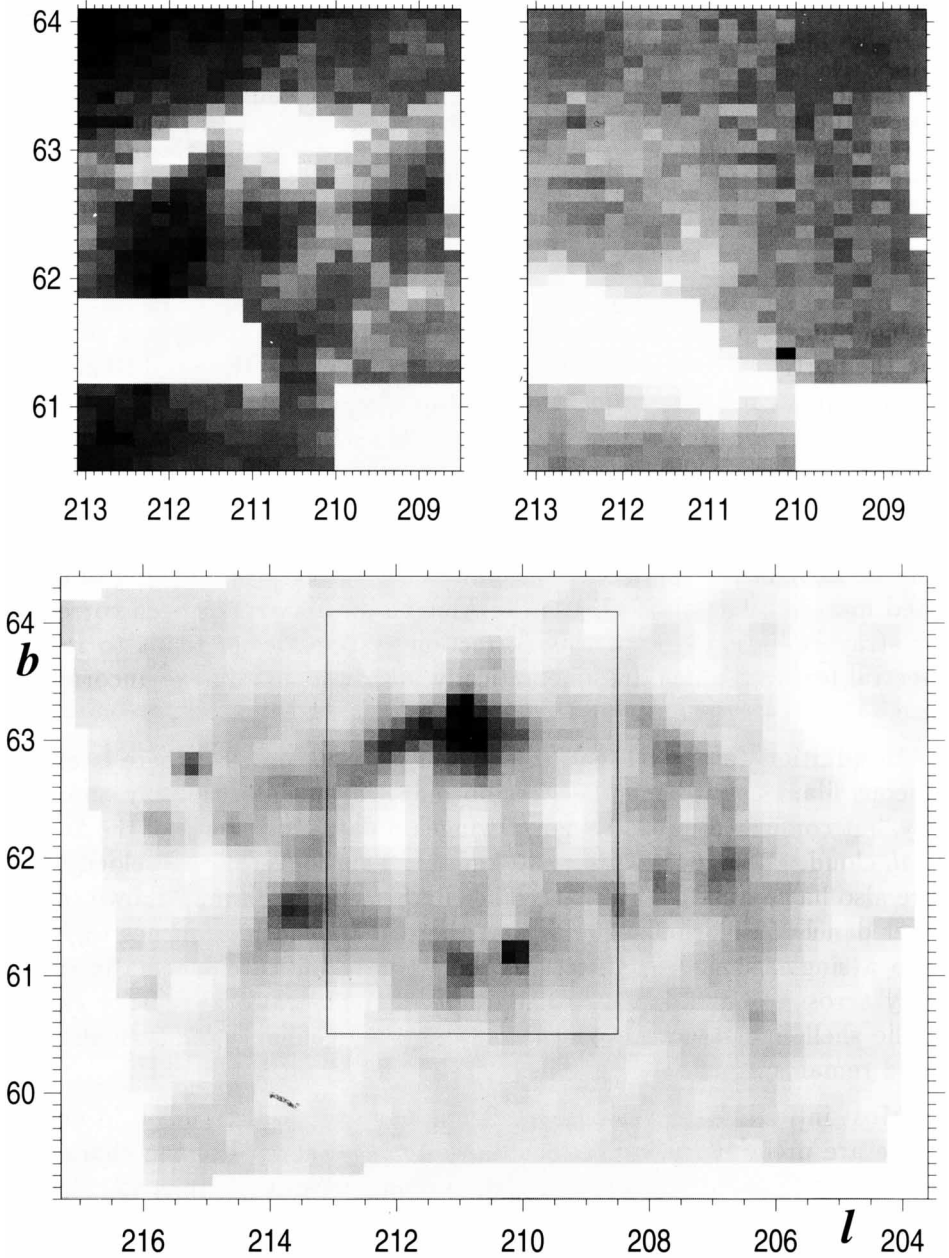
Figure 9. HI column densities, measured at Arecibo (West *et al.* 1995), corresponding to λ21–cm emission from the range -50 km s$^{-1} \leq v \leq -30$ km s^{-1} (left) and from the range -10 km s$^{-1} \leq v \leq +10$ km s^{-1} (right), compared with the IRAS 100–micron flux in the lower panel. (The boxed region in the lower panel delineates the extent of the Arecibo data.) The anomalous–velocity HI feature is correlated with a dust cirrus counterpart centered near $(l, b) = (211°, 63°)$; the strength of the HI emission at conventional velocities is, in this region, weaker than that of the peculiar–velocity material. (Higher fluxes are whiter in the HI case, but blacker in the IR representation.)

The matter of the characteristic distance to the IVC structures remains elusive. (Distances to HVCs are also only poorly established, but the particular importance of the IVC distances is emphasized by their clear association with cirri, which may be the principal carrier of the interstellar medium, and with perturbances in the conventional gas layer.) Substantial efforts have been directed to the detection of interstellar absorption lines in the directions of stars lying beyond IVC structures. Danly (1989) found ultraviolet absorption lines at about -50 km s^{-1} towards stars whose distances were evidently large, between 400 and 700 pc, but not towards stars nearer by.

Acceptance of distances of the order of 500 pc as being generally typically of the intermediate–velocity–cloud objects has a number of consequences. Such a characteristic distance is not compatible with the value of the vertical thickness of the galactic gas layer measured over much of the distant Galaxy. Values for the vertical thickness, measured as the Gaussian dispersion, σ_z, perpendicular to the galactic equator, are typically about 120 pc for both the HI and the dust layer radiating at 100–micron, and about half this value for the molecular–cloud ensemble. If the IVC HI gas (and the dust which at least to some extent is associated with that gas) were to be as distant as 400 to 700 pc, then the layer–thickness measures would have been larger, unless the IVC gas were confined to a very peculiar distribution. This peculiar distribution would involve two vertical, narrow cones with their vertices pointing toward the Sun. In other words, if the IVCs are quite distant, then they are, ironically, probably a *local* phenomenon, not a general aspect of the galactic gas layer. (Such localized HI disturbances have been seen in other galaxies.)

Acceptance of a large characteristic distance for the IVC gas led Lockman and Gehman (1991) to reject velocities $|v| \geq 30$ km s^{-1} from their discussion of the role of turbulence in the lower–halo gas. If the scale–thickness argument requires a smaller characteristic distance, then the turbulence of entities populating the IVC regime would in fact play an important role in the galactic–layer energetics. The motions in the lower–halo gas layer would then better be viewed in terms of turbulence of an ensemble of separate entities rather than in terms of high–dispersion wings from a diffuse gas component. We note that the anomalous velocities of the IVCs and their associated dust cirri are dominated by motions in the sense of infall, and are thus, in this regard, not indicative of normal turbulence. We note also that the measured motions are *vertical* ones, which evidently have no *horizontal* equivalent, at least at low $|b|$; measures of the bulk–motion turbulence at low $|b|$ are characterized by random–motion dispersions of less than about 5 km s^{-1}.

$+18 \leq V_{rad} \leq +20$ km s^{-1}
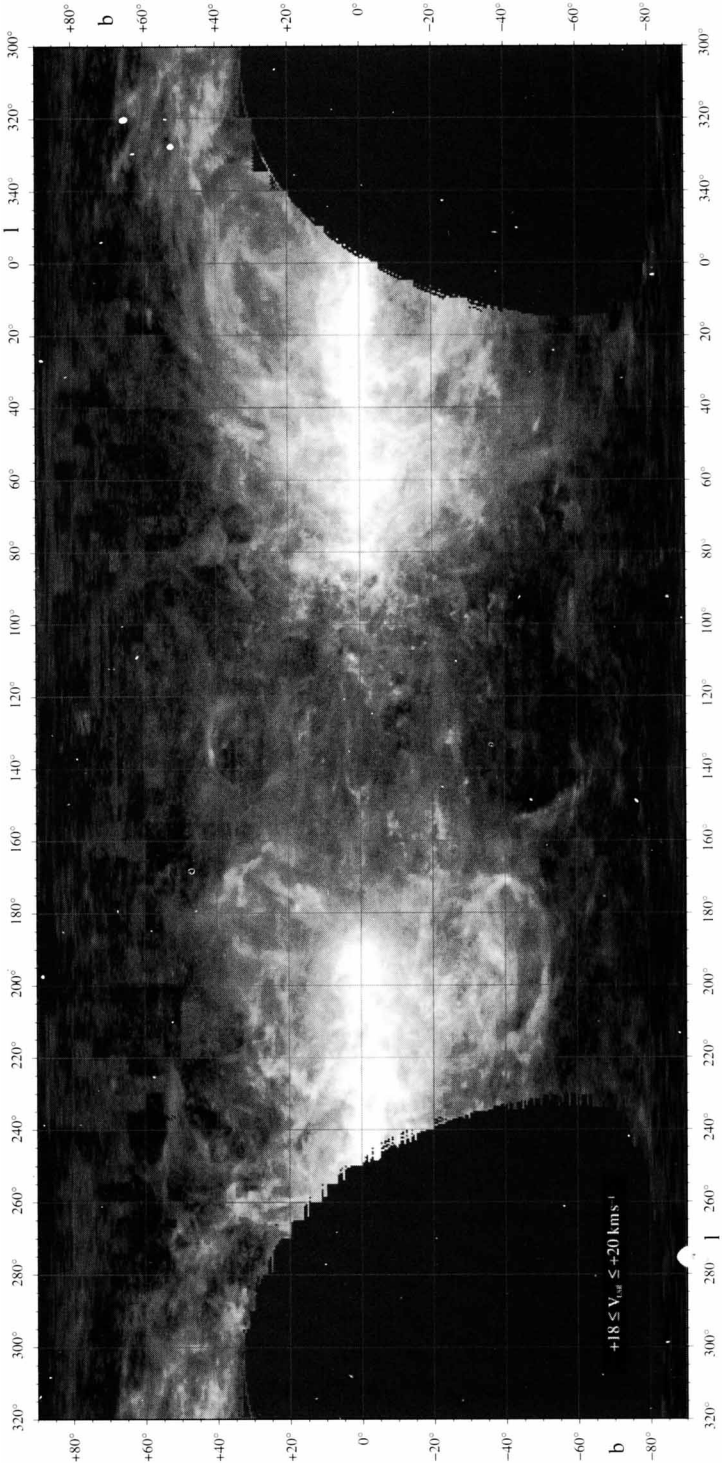
Figure 10. Distribution over the plane of the sky of HI column depths contributed over the narrow velocity range $+18$ km s^{-1} $\leq v \leq +20$ km s^{-1}. Much of the HI gas is   marshaled into filamentary structures such as that associated with the Orion/Eridanus bubble, and many of these cover a large total velocity expanse, implying substantial energetics. $\Longleftarrow$

[Gray Scale] HI: $+13.5 \leq v_{LSR} \leq +18.5$ km/s;   [Contours] X-ray: L1 band
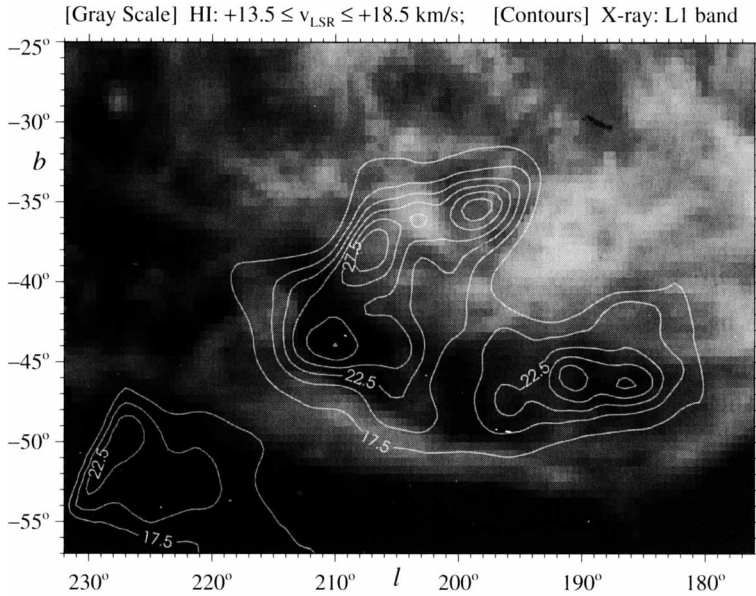
Figure 11. Confinement of 1/4 keV X–ray emissivities (from Burrows *et al.* 1992, shown by contours) by HI structures associated with the Orion/Eridanus bubble (Brown *et al.* 1995). The Orion OB1 association has caused a cavity filled with hot gas, surrounded by an expanding shell of HI. Comparison with the HI data in the range $+13.5$ km s^{-1} $\leq v \leq +18.5$ km s^{-1} shows an anticorrelation of the X–ray enhancement with kinematically–narrow HI features.

The sky–image moment map shown in Figure 10 represents the narrow positive–velocity range $+18$ km s^{-1} $\leq v \leq +20$ km s^{-1}. The most prominent of the remarkable structures seen in this image is the large shell–like Orion/Eridanus bubble, centered near $(l, b) = (200°, -40°)$. This feature is a prototypical example of the marshaling of various aspects of the kinematics and structure of the interstellar medium by consequences of star formation. HI and X–ray data from the region lead to a picture of a cavity filled with hot gas, surrounded by an expanding shell of neutral material. The HI material provides important information on the kinematics of the expanding shell.

Figure 12.   Distribution over the plane of the sky of HI column depths contributed over the velocity range $+80$ km s^{-1} $\leq v \leq +90$ km s^{-1}. Comparison of this velocity slice with the one at complementary negative velocities shown in Figure 4 shows the well–known, but poorly understood, $+/-$ kinematic asymmetry; there is also an obvious north/south asymmetry. The first galactic quadrant at these velocities displays some evidently violent ejecta; the third quadrant is populated by a number of high–velocity clouds, which generally are relatively scarce at positive velocities.

$\Longrightarrow$

Brown *et al.* (1995) show a sequence of maps from the Leiden/Dwingeloo survey which indicate that the neutral hydrogen emission from the area surrounding the Orion/Eridanus bubble spans a total velocity extent of some 80 km s^{-1}. The enhanced X–ray flux in that area anticorrelates in a detailed way with narrow–dispersion HI features, clearly establishing the association of the X–ray enhancement with the bubble. Using models for wind–blown bubbles which incorporate the density stratification of the galactic HI layer, Brown *et al.* show that the Orion/Eridanus structure can be explained as a bubble blown by winds from Orion OB1.

The last moment–map image shown here is that in Figure 12 representing the HI emission from the positive–velocity interval $+80$ km s^{-1} $\leq v \leq +90$ km s^{-1}. Comparison of this image with the one at complementary negative velocities shown in Figure 4 indicates the kinematic asymmetry characterizing the HVC and IVC gas. High–velocity–cloud objects occur sparsely at positive velocities (see the review by Wakker, 1991); the positive–velocity HVC objects represented in this image in the third galactic quadrant differ also from those at complementary negative velocities in being quite isolated features, spanning angular scales typically less than 5°, rather than extended complexes spanning many tens of degrees. The features at anomalously–high positive velocities do share, however, the preference for positive latitudes shown by the negative–velocity HVCs.

The Figure 12 image also illustrates, in the first quadrant, several of the characteristic HI structures (variously called "worms", "chimneys", etc.) which appear to be associated with disturbances in the galactic–equator gas layer. Such disturbances are currently being studied by a number of groups; the nature of the responsible disturbance is still puzzling. Just as is the case at negative velocities, disturbances to the conventional gas layer may distort derived parameters such as the scale thickness. We note that these disturbances are *vertical* ones. The terminal–velocity cutoff of HI spectra at $b = 0°$ is a good kinematic measure of the line–of–sight *horizontal* turbulence; this measure constrains peculiar motions in the galactic equator to be quite small, with excursions away from the expected terminal velocity seldom greater than about 5 km s^{-1}.

$+80 \leq V_{LSR} \leq +90$ km s^{-1}
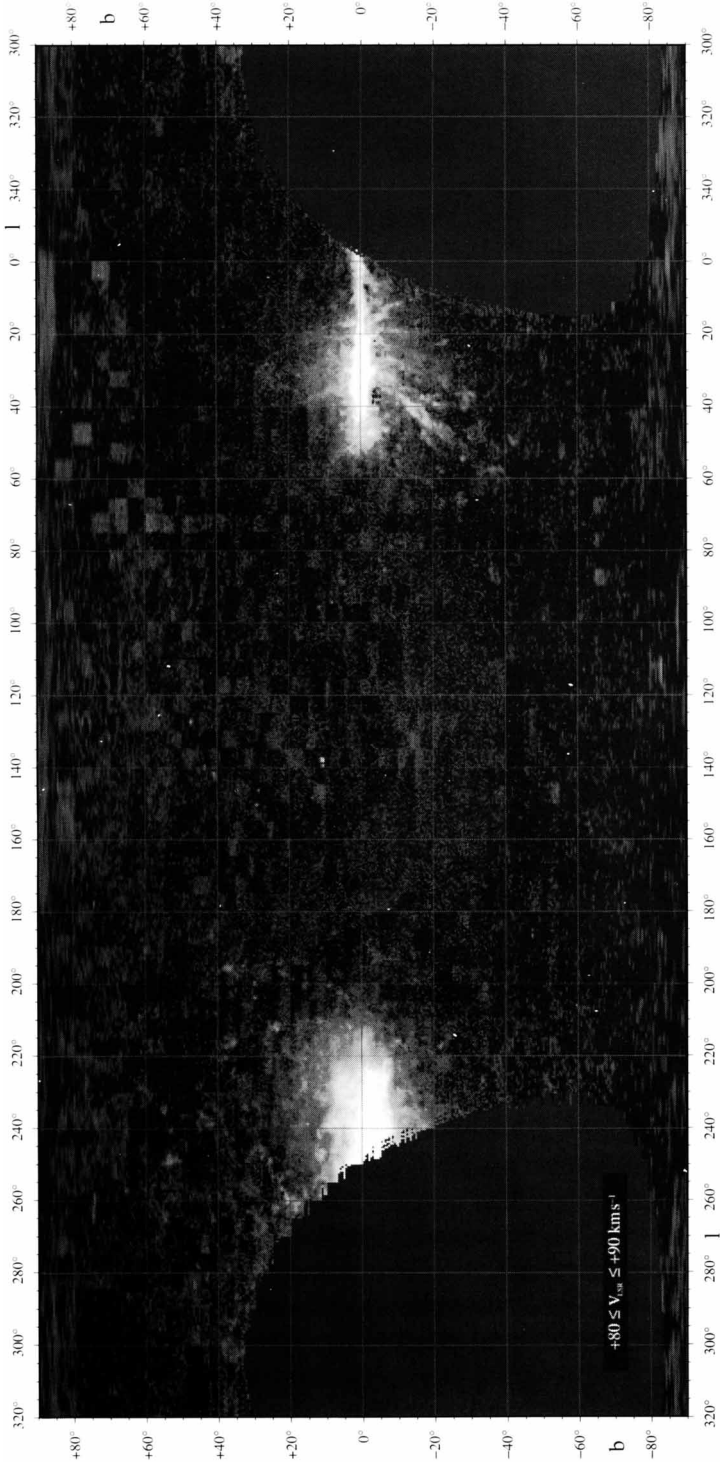
The survey material is being published as an atlas of maps and as a FITS–format data cube on a CD–ROM (Hartmann and Burton, 1996).

The Leiden/Dwingeloo survey covers the sky accessible from the Netherlands. Southern extension of the coverage to include the region $\delta \leq -30°$ is underway at the Argentina Institute for Radioastronomy, where E. Bajaja and collaborators are using the 100–foot IAR telescope equipped with a receiver and spectrometer comparable to those used in Dwingeloo.

The Dwingeloo radio telescope is operated by the Netherlands Foundation for Research in Astronomy, under contract with the Netherlands Organization for Scientific Research. The Arecibo radio telescope is operated by the National Astronomy and Ionosphere Center, under contract with the U.S. National Science Foundation.

References

Brown, A.G.A., Hartmann, D., and Burton, W.B. (1995), *Astron. Astrophys.*, submitted.

Burrows, D.N., Singh, K.P., Nousek, J.A., Garmire, G.P., and Good, J. (1993), *Astrophys. J.* 406, 97.

Burstein, D. and Heiles, C. (1978), *Astrophys. J.* 225, 40.

Burton, W.B. (1992), in *The Galactic Interstellar Medium*, (D. Pfenniger & P. Bartholdi, eds.), Springer-Verlag, Heidelberg, p. 1.

Burton, W.B., Bania, T.M., Hartmann, D., and Tang, Y. (1992), in *Evolution of Interstellar Matter and Dynamics of Galaxies*, (J. Palous, W.B. Burton, & P.O. Lindblad, eds.), Cambridge University Press, Cambridge, p. 25.

Danly, L. (1989), *Astrophys. J.* 342, 785.

Deul, E.R., and Burton, W.B. (1990), *Astron. Astrophys.* 230. 153.

Désert, F.-X., Bazell, D., and Blitz, L. (1990), *Astrophys. J. Letters*, 355, L51.

Dickey, J.M., and Lockman, F.J. (1990), *Ann. Rev. Astron. Astrophys.*, 28, 215.

Hartmann, D. (1994), *The Leiden/Dwingeloo Survey of Galactic Neutral Hydrogen*, Ph.D. Thesis, University of Leiden.

Hartmann, D., and Burton, W.B. (1996), *An Atlas of Galactic Neutral Hydrogen*, Cambridge University Press, in press.

Hartmann, D., Kalberla, P.M.W., Burton, W.B., and Mebold, U. (1995), *Astron. Astrophys.*, submitted.

Hartsuijker, A.P., Baars, J.W.M., Drenth, S., and Gelato–Volders, L. (1972), *IEEE Trans. Antennas Propagation* 20, 166.

Heiles, C., and Habing, H.J. (1974), *Astron. Astrophys. Suppl.* 14, 1.

Heiles, C., Reach, W.T., and Koo, B.–C. (1988), *Astrophys. J.* 332, 313.

Herbstmeier, U., Mebold, U., Snowdon, S.L., Hartmann, D., Burton, W.B., Moritz, P., Kalberla, P.M.W., and Egger, R. (1995), *Astron. Astrophys.*, in press.

Kalberla, P.M.W., Mebold, U., and Reich, W. (1980), *Astron. Astrophys.* 82. 275.

Lockman, F.J. and Gehman, C., (1991), *Astrophys. J.* 382, 182.

Lockman, F.J., Jahoda, K., and McCammon, D. (1986), *Astrophys. J.* 302, 432.

Mebold, U., Herbstmeier, U., Kalberla, P.M.W., Souvatzis, I. (1989), in *Structure and Dynamics of the Interstellar Medium*, (G. Tenorio–Tagle, M. Moles, and J. Melnick, eds.), Springer Lecture Notes in Physics, p. 424.

van Someren Greve, H. (1991), in *Proc. Workshop "Holography Testing of Large Radio Telescopes"*, Nauka, Leningrad.

Wakker, B.P. (1991), *Astron. Astrophys.* 250, 499.

West, S.R.D., Burton, W.B., Hartmann, D., Bania, T.M., and Stark, R. (1995), in preparation.